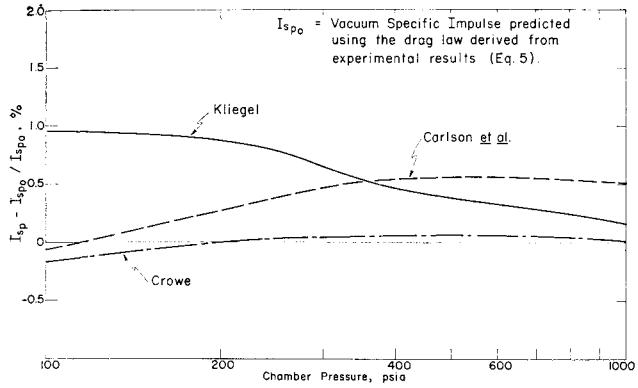

Fig. 2 Percentage error in vacuum specific impulse resulting from the use of the devised drag laws.

lowing empirical expression was developed to best fit the data,

$$\bar{C}_D = \frac{1.1}{1 + 1.1Kn^{-0.3}\exp(-Kn^{1/2})} \times \left\{1 - \exp\left[-Kn^{0.7}e^{Kn}\frac{(C_{D0} - 0.48)Re}{6.6}\right]\right\} \quad (5)$$

The purpose of the Note is to demonstrate the effect on nozzle performance predictions of using the drag laws devised before data were available. The calculations were performed using a computer program[1] for one-dimensional two-phase flow with chamber conditions typical of a solid-propellant motor and chamber pressures ranging between 100 and 1000 psia. Mass median particle sizes as measured by tank collection tests[1] from subscale motors were used in the calculations at the various pressure levels. Vacuum specific impulses of a nozzle with a 40:1 expansion ratio and a 1.2-in. diam. throat were calculated employing the various drag laws.

The percentage difference in nozzle performance predictions resulting from using each devised drag law and that validated by experiment [Eq. (5)] is illustrated in Fig. 2. At low-pressure levels the drag law used by Kliegel leads to a performance prediction which is 1% too high whereas the use of the other two drag laws results in very small differences in performance prediction. At the high-pressure levels, where rarefaction effects are less significant, Carlson's law results in the least accurate prediction although still less than 0.5%. Performing the same calculations for larger nozzles shows that the choice of drag law has even less effect on performance predictions because of reduced two-phase flow losses with increased nozzle scale.

Using the drag coefficient for a sphere in incompressible flow as the drag law in the flow analysis of the same nozzle considered previously results in a vacuum specific impulse which is 3.7% too high at a chamber pressure of 100 psia. An inaccuracy of this magnitude would lead to an intolerable 10–12 point error in the specific impulse prediction of a high-performance low-pressure motor to operate in a space environment, thereby showing the importance of accounting for flow-rarefaction effects.

In conclusion, the drag laws devised before data were available to account for rarefaction effects have not led to large errors in specific impulse predictions. Thus discrepancies between predicted and measured nozzle performance which, in the past, were attributed to lack of knowledge of the particle drag coefficient were likely a result of the still unresolved problem of condensed-phase particle size.

References

[1] "Dynamics of Two-phase Flow in Rocket Nozzles," UTC 2102-FR, Sept. 1965, United Technology Center, Sunnyvale, Calif.

[2] Carlson, D. J. and Hogland, R. F., "Particle Drag and Heat Transfer in Rocket Nozzles," *AIAA Journal*, Vol. 2, No. 11, Nov. 1964, pp. 1980–1984.

[3] "Measurement of Particle Drag Coefficients in Flow Regimes Encountered in a Rocket Nozzle," UTC 2296-FR, March 1969, United Technology Center, Sunnyvale, Calif.

[4] Miller, W. H. and Barrington, D. K., "A Review of Contemporary Solid Rocket Motor Performance Prediction Techniques," *Journal of Spacecraft and Rockets*, Vol. 7, No. 3, March 1970, pp. 225–237.

[5] Gilbert, M., Davis, L., and Altman, D., "Velocity Lag of Particles of Linearly Accelerated Combustion Gases," *Jet Propulsion*, Vol. 25, No. 1, 1955, pp. 26–30.

[6] Kliegel, J. R., "Gas Particle Nozzle Flows," *Ninth International Symposium on Combustion*, Academic Press, 1963, pp. 811–827.

[7] Millikan, R. A., "The General Law of Fall of a Small Spherical Body Through a Gas, and Its Bearing upon the Nature of Molecular Reflection from Surfaces," *The Physical Review*, Vol. 22, 1923, pp. 1–23.

[8] Crowe, C. T., "Drag Coefficient of Particles in a Rocket Nozzle," *AIAA Journal*, Vol. 5, No. 5, May 1967, pp. 1021–1022.

[9] Sherman, F. S., "A Survey of Experimental Results and Methods for the Transition Regime of Rarefied Gas Dynamics," *Rarefied Gas Dynamics*, Vol. 2, Supplement 2, Academic Press, 1963, pp. 228–259.

[10] "Fundamentals of Gas Dynamics," *High-Speed Aerodynamics and Jet Propulsion*," Vol. 3, Princeton University Press, 1958, p. 704.

[11] Liu, C. V. and Sugimura, T., "Rarefied Gas Flow of a Sphere at Low Mach Numbers," *Rarefied Gas Dynamics*, Vol. 1, Supplement 5, Academic Press, 1969, pp. 789–796.

Modification of Radiant Enclosure Equations for Third Generation Digital Computers

JIMMIE H. SMITH*
Sandia Laboratories, Albuquerque, N. Mex.

Nomenclature

NTEMP	=	number of surfaces with specified temperature
NFLUX	=	number of surfaces with specified heat flux
NS	=	NFLUX + NTEMP = total number of surfaces in enclosure
A_i	=	surface area i
F_{ij}	=	geometric view factor from surface i to j
B_i	=	radiosity or total flux leaving surface i
T_i	=	temperature of surface i
ϵ_i	=	emissivity of surface i
Q_i	=	heat flux to surface i
δ_{ij}	=	Kronecker delta = 0 if $i \neq j$; 1 if $i = j$
σ	=	Stefan-Boltzmann constant
ψ(INDEX)	=	element of symmetric-matrix inverse
INDEX	=	equivalent one-dimensional subscript replacing i and j

Introduction

MODERN literature on radiation heat transfer derives and uses the equations of radiant interchange in matrix form for solution on digital computers. These equations generally are not written to use minimum core storage. Yet, two compelling reasons dictate that this requirement be met. One is

Received September 28, 1970; revision received September 28, 1970. This work was done under the auspices of the United States Atomic Energy Commission.

* Applied Mathematician-Scientific Programer, currently at University of Texas on educational leave from Sandia Laboratories.

that current defense industry problems involving multimode heat transfer often need more than the available core. A less well-known reason is far more often significant. The latest digital computers, such as the CDC-6600 and the UNIVAC 1108 with EXEC VIII, use multiprogramming; the available core is no longer dedicated to a single user at a time, but rather, is shared among several. Hence, penalty algorithms decrease priority inversely with both estimated run time and core requirement; even programs with short run times will be run less often if they extravagantly reserve more core than needed.

As an example, we take the usual equations of radiant interchange between gray and diffuse emitting and reflecting enclosure surfaces. Then each of these doubly subscripted nonsymmetric equations is converted to an equivalent singly subscripted symmetric form. These modifications are simple in principle. They are presented here to obviate their repetition by countless other users.

Algorithm for Using Upper Triangular and Main Diagonal View Factor Matrix

In storing an $NS \times NS$ matrix we need NS^2 locations. But in storing only the main diagonal and upper triangle, we need a lesser number, as follows: The first row has NS elements, the second row has $(NS - 1)$ elements, and so on. Each row has one element less than the one above it until, finally, the last row contains exactly one element. Thus, the sum consists of $NS + (NS - 1) + (NS - 2) + \ldots + 1$. This is an arithmetic progression whose first term is NS and whose last term is 1, and the difference between terms is 1. The number of terms is NS. The sum is $(NS/2)(NS + 1)$. In a digital computer, the division by 2 must be done last to avoid any intermediate noninteger values which would be truncated. $NS(NS + 1)$ is always even.

Now consider an algorithm for converting two-dimensional row and column coordinates into a one-dimensional index, as follows: The one-dimensional index must count the upper half matrix. The count will proceed left to right across the first row, up to NS elements. Then, on each succeeding row, going downward, the count is left to right. However, the first element to be counted on any row is the main diagonal element. Thus, the index to any arbitrary element (i,j) is

$$\text{INDEX} = NS + (NS - 1) + (NS - 2) + \ldots + [NS - (i - 2)] + [j - (i - 1)] \quad (1)$$

where $j \geq i$ to obtain upper triangle and main diagonal;

$$\text{INDEX} = NS(1 + i - 2) - [1 + 2 + \ldots + (i - 2)] + j - i + 1$$

Again we sum an arithmetic progression to get

$$\text{INDEX} = NS(i - 1) - (i - 2)[(i - 2) + 1]/2 + j - i + 1 \quad (2)$$

Finally, after manipulation,

$$\text{INDEX} = [(i - 1)(2*NS - i)/2] + j \text{ for } j \geq i \quad (3a)$$

$$\text{INDEX} = [(j - 1)(2*NS - j)/2] + i \text{ for } j < i \quad (3b)$$

With either form of INDEX, division by 2 must be the last operation in the left term of the right side. Otherwise, truncation errors may occur. Equation (3b) generates the lower triangular matrix as a reflection of the upper triangle about the main diagonal.

Symmetric Interchange Equations

It would serve no purpose to repeat the well-known gray enclosure energy balances here. Instead, we begin each modification with two standard equations by Sparrow and Cess.[1] A reader may then check the basis of either starting equation here in the well-known and excellent textbook (Ref. 1).

The equations of Sparrow and Cess give matrix elements which contain the geometric view factor without its corresponding area. Thus, the Sparrow and Cess equations indicate storage and inversion of full nonsymmetric matrices, since $F_{ij} \neq F_{ji}$ in general. Reciprocity suggests that since $A_iF_{ij} = A_jF_{ji}$, we may be able to scale the Sparrow and Cess equations to obtain symmetric matrices. We succeed in two cases out of three. That is, if either all of the temperatures or all of the heat fluxes are given, we then create a symmetric matrix which is easier to store and invert. Only if a mixture of temperatures and fluxes are given must we store and invert a nonsymmetric matrix. Moreover, we will develop an algorithm such that only the main diagonal and upper triangle of the view factor matrix is ever stored. By knowing areas and by using reciprocity, we can always deduce the missing view factors.

All temperatures specified

Equation (3-23) of Sparrow and Cess is

$$\sum_{j=1}^{NTEMP} \left[\frac{\delta_{ij} - (1 - \epsilon_i)F_{ij}}{\epsilon_i} \right] B_j = \sigma T_i^4 \quad (4)$$

The B_j's are the unknown radiosities and their multipliers are the nonsymmetric coefficients of the matrix to be inverted. To obtain symmetry, the off-diagonal terms, $(1 - \epsilon_i)/(\epsilon_i)F_{ij}$ must become A_iF_{ij}. Therefore, we multiply Eq. (4) by $A_i\epsilon_i/(1 - \epsilon_i)$ and insert INDEX

$$\sum_{j=1}^{NTEMP} \left[\frac{\delta_{ij}A_i}{1 - \epsilon_i} - A_iF(\text{INDEX}) \right] B_j = \frac{A_i\epsilon_i}{1 - \epsilon_i} \sigma T_i^4 \quad (5)$$

With the coefficients of B_j defined in this symmetric manner, we do a symmetric matrix inversion to find the inverse elements, $\psi(\text{INDEX}) = [\delta_{ij}A_i/(1 - \epsilon_i) - A_iF(\text{INDEX})]^{-1}$.

$$B_i = \sum_{j=1}^{NTEMP} \psi(\text{INDEX}) \frac{A_i\epsilon_i}{1 - \epsilon_i} \sigma T_i^4 \quad (6)$$

$$Q_i = (\sigma T_i^4 - B_i)A_i\epsilon_i/(1 - \epsilon_i) \quad (7)$$

All heat fluxes specified

From Eq. (3–32) of Sparrow and Cess we get, after rearranging,

$$\sum_{j=NTEMP+1}^{NS} (\delta_{ij} - F_{ij})B_j = \frac{Q_i}{A_i} \quad (8)$$

Noting that, in this case, $NTEMP + 1 = 1$ and $NS = NFLUX$ = number of given heat fluxes, we multiply Eq. (8) by A_i to obtain symmetry and insert INDEX

$$\sum_{j=1}^{NFLUX} [A_i\delta_{ij} - A_iF(\text{INDEX})]B_j = Q_i \quad (9)$$

Again we perform a symmetric matrix inversion to find the inverse elements $\psi(\text{INDEX}) = [A_i\delta_{ij} - A_iF(\text{INDEX})]^{-1}$.

$$B_i = \sum_{j=1}^{NFLUX} \psi(\text{INDEX})Q_i \quad (10)$$

$$T_i = \{[B_i + Q_i(1 - \epsilon_i)/\epsilon_iA_i]/\sigma\}^{1/4} \quad (11)$$

Note that with a mixture of specified temperatures and heat fluxes, there is no way to achieve symmetry. In this event, employing the usual equations in the literature is the best one can do, except that the view-factor matrix may still be treated as symmetric.

Also note that Eqs. (6) and (10) depend on the theorem that a nonsingular symmetric matrix has a symmetric inverse.

Results

The modified equations derived here were programmed and used in conjunction with the transient heat equation with source term. The radiant heat to each node was input in the source term after each conduction time step. This quasi-linearization of the combined transient conduction and radiation problems gave credible results.

In a problem with constant emissivities, only one symmetric matrix inversion was required for all of these equations. However, in a problem where emissivities varied with temperature, this inversion was required after each conduction time step. Even a symmetric matrix inversion proved too time consuming. The equations derived here were solved by a less accurate relaxation technique for this case.

The largest problem solved contained 300 enclosure surfaces. The core saving was $300^2 - (300/2)(300 + 1) = 44{,}850_{10}$ words. The time saved by a symmetric vs a nonsymmetric system of equations is difficult to estimate precisely. However, considering that the solution is performed thousands of times per computer run when emissivity varies with temperature, the savings can be quite significant.

Reference

[1] Sparrow, E. M. and Cess, R. D., *Radiation Heat Transfer*, Brooks Cole Publishing Co., Belmont Calif., 1966.

Propellant Condensation on Surfaces near an Electric Rocket Exhaust

W. C. Lyon*
Hittman Associates, Inc., Columbia, Md.

In a recent paper,[1] Reynolds and Richley considered propellant condensation near the exhaust of ion thrusters. In part, they stated, "Charge exchange ions formed in the exhaust beam are not collimated and their scattering and impaction on surrounding surfaces could be a problem. However, both the quantity and energy levels are considerably less than those of the primary ions.[2] Because of the magnitude of neutral efflux and the lack of collimation, neutral particle effluxes present a potentially more serious problem." This conclusion is identical to that of Staggs, et al.[2] Recently, we completed an investigation in which the charge exchange mechanism could cause condensation or erosion problems where the primary beam and neutral fluxes constituted no problem. The data reinforce the first part of the Reynolds and Richley conclusion and point out the potential danger in neglecting small contributors.

The application investigated[3] is illustrated in Fig. 1. It consists of a cylindrical spacecraft with a cesium ion thruster thrusting at 45° to the spacecraft axis. Located in the same plane is a radiator with a cold patch designed to operate at 100°K. The geometry prohibits direct impacting of the neutral atoms (or Group 2 ions) upon the cold patch, but Group 4 ions have a direct entry to the patch.

Neutral Atom Distribution

The neutral atom distribution for $r > a$, is approximately[4]

$$\Gamma(r,\theta) = \Gamma_0 \frac{a^2}{r^2} \cos\theta \Big/ \left[1 + \frac{2a^2}{r^2}\cos\theta + \frac{a^4}{r^4}\right]^{1/2} \qquad (1)$$

Received April 13, 1970; revision received July 16, 1970. This work was performed under NASA-GSFC Contract NAS5-9479, Modification 14.

* Staff Consultant. Member AIAA.

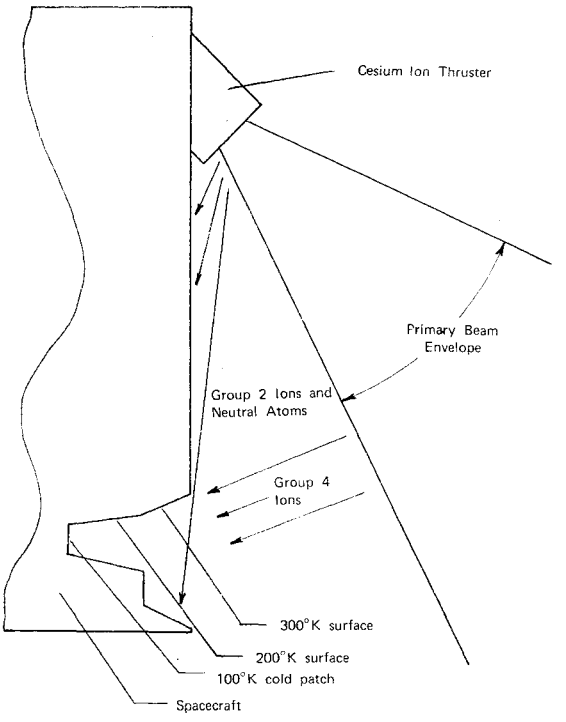

Fig. 1 Approximate spacecraft-thruster configuration showing low temperature radiator.

where Γ is the particle current density in the direction of the radius vector; r is the distance from the center of the ion engine exhaust plane to the position of interest; θ is the angle between r and the normal to the engine exhaust plane; Γ_0 is the particle current density at the ion engine exhaust plane; and a is the radius of the ion engine exhaust opening.

The assumed thruster† has an atomic (un-ionized) flow rate of 10^{-7} lb/sec of cesium. For the geometry considered, the direct neutral flux arriving on the lower 300°K surface is about 2.3×10^{12} atoms/cm²-sec. This temperature is high enough that the atoms do not accumulate, but immediately evaporate.‡ The approximate distribution of atoms which results is given in Table 1. The cold patch does not "see" a 300°K surface and consequently no cesium arrives at the cold patch from such surfaces.

The evaporation rate for a surface at 200°K is 7.1×10^7 atoms/cm²-sec. Hence, for practical purposes, the cesium accumulation rate on this surface is equal to the rate at which cesium atoms arrive if one assumes a sticking coefficient of

Table 1 Approximate distribution of atoms to surfaces and space

Destination	Percentage of atoms hitting lower 300°K surface	Arrival flux, atoms/cm²-sec
Upper surface at 300°K	12.2	1.1×10^{11}
Upper surface at 200°K	7.5	1.3×10^{11}
Radiator side walls at 300°K (not shown in Fig. 1)	20.2	...
Space	60.1	...

† The calculations are based upon behavior assumed by the author and R. Hunter (NASA-GSFC). See Ref. 5 for a description of a typical cesium thruster.

‡ Evaporation rate is calculated from[3] $N = P/(2\pi mkT)^{1/2}$, where P is the vapor pressure, m the mass of the atom, k the Boltzmann constant, and T the absolute temperature.